Available online at www.sciencedirect.com
ScienceDirect
Journal of Nuclear Materials 367–370 (2007) 251–256
journal of nuclear materials
www.elsevier.com/locate/jnucmat

Molecular dynamics modelling of radiation defects in ferromagnetic α-iron

S.L. Dudarev [a,*], P.M. Derlet [b]

[a] EURATOM/UKAEA Fusion Association, Culham Science Centre, Oxfordshire OX14 3DB, UK
[b] Paul Scherrer Institute, CH-5232 Villigen PSI, Switzerland

Abstract

The need to perform large-scale molecular dynamics simulations of radiation defects in ferritic steels has stimulated the recent development of a 'magnetic' interatomic potential for body-centred cubic α-iron [1,2]. Here we describe the first application of the new method to molecular dynamics modelling of radiation defects. We investigate the magneto-elastic fields of defects and study their thermally activated migration. We propose that the origin of the low-temperature ($T \leqslant 120$ K) resistivity recovery stages in irradiated α-iron is associated with clustering of self-interstitial atoms.

1. Introduction

Magnetism has significant implications for the structural stability of materials. Equilibrium positions of atoms depend sensitively on magnetic ordering in the case where the magnetic energy and the difference between energies of competing crystal phases are of the same order of magnitude. This was noted by Hasegawa and Pettifor [3] who showed that magnetism stabilizes the body-centred cubic (bcc) α-phase of iron. Thermal magnetic fluctuations are responsible for the phase transition from the bcc α to the fcc γ phase occurring at approximately 912 °C.

So far the analysis of the relationship between structural and magnetic properties was focused on the treatment of spatially homogeneous crystalline solids. It excluded the case of strong localized lattice deformations, for example point defects and dislocations, which are essential for predictive modelling of materials for fusion and advanced nuclear applications.

In this paper we give a brief summary of a new approach to molecular dynamics simulations of magnetic iron. This approach is based on a combination of the Stoner model treatment of band ferromagnetism [4] and the Ginzburg–Landau model [5]. The latter is the simplest model of a second-order phase transition, and it provides a convenient means for evaluating the energy of symmetry-broken magnetic solutions. By combining the Stoner and the Ginzburg–Landau models we are able to derive the functional form of the magnetic part of the many-body interatomic potential [1,2] and

* Corresponding author. Tel.: +44 1235 466513; fax: +44 1235 466435.
E-mail addresses: Sergei.Dudarev@UKAEA.org.uk (S.L. Dudarev), Peter.Derlet@psi.ch (P.M. Derlet).

0022-3115/$ - see front matter © 2007 Elsevier B.V. All rights reserved.
doi:10.1016/j.jnucmat.2007.03.009

parameterize it in the form suitable for large-scale molecular dynamics simulations.

Here we consider several applications of the new method. We investigate magneto-elastic fields associated with radiation-induced defects and dislocation loops in ferromagnetic α-iron. We also study the dynamics of migration of radiation-induced defects in iron and show that, depending on the compactness of a self-interstitial atom (SIA) cluster, the interstitial atoms may form local ⟨1 1 0⟩-like groups impeding thermally activated mobility of clusters at low temperatures. We discuss implications of these findings for the treatment of cascade damage effects under neutron irradiation. Our findings suggest that the very low-temperature ($T \leqslant 120$ K) recovery stages in irradiated α-iron are likely associated with the formation of mobile clusters of self-interstitial atoms.

2. Effect of magnetism on interatomic interactions

Ferromagnetism in bcc iron results from a combined effect of on-site electron exchange and correlations, and quantum inter-site hopping of 3d-electrons. Hopping of electrons in the bcc lattice of iron gives rise to the formation of a ∼6 eV wide d-band characterized by the distribution of the density of states $D(E)$ shown in Fig. 1. The fact that in the non-magnetic state the Fermi energy is at a maximum of the density of states gives rise to the Stoner instability, and to the formation of a symmetry-broken low-energy ferromagnetic state of the material. The total energy of band electrons (per atom) in the Stoner model is given by

$$E_{\rm tot} = \int_{-\infty}^{\epsilon_{\rm F\uparrow}} ED(E)\,{\rm d}E + \int_{-\infty}^{\epsilon_{\rm F\downarrow}} ED(E)\,{\rm d}E - I\zeta^2/4, \tag{1}$$

where the distribution of the density of states $D(E)$ is shown in Fig. 1, I is the Stoner parameter, $\epsilon_{\rm F\uparrow}$ and $\epsilon_{\rm F\downarrow}$ are the Fermi energies of spin up and spin down sub-bands. ζ is the magnetic moment per atom given by the difference of the occupation numbers of spin up and spin down states

$$\zeta = \int_{-\infty}^{\epsilon_{\rm F\uparrow}} D(E)\,{\rm d}E - \int_{-\infty}^{\epsilon_{\rm F\downarrow}} D(E)\,{\rm d}E = \int_{\epsilon_{\rm F\downarrow}}^{\epsilon_{\rm F\uparrow}} D(E)\,{\rm d}E. \tag{2}$$

In the limit $|\zeta| \ll 1$ Eq. (1), subject to the charge neutrality condition

$$N = \int_{-\infty}^{\epsilon_{\rm F\uparrow}} D(E)\,{\rm d}E + \int_{-\infty}^{\epsilon_{\rm F\downarrow}} D(E)\,{\rm d}E = {\rm const.}, \tag{3}$$

can be approximated by the expression

$$E_{\rm tot}(\zeta) = E_{\rm tot}(0) + \left[\frac{1}{D(\epsilon_{\rm F})} - I\right]\frac{\zeta^2}{4} + \cdots, \tag{4}$$

where $\epsilon_{\rm F}$ is the Fermi energy of the non-magnetic ($\zeta = 0$) state. If $D(\epsilon_{\rm F})I > 1$ the non-magnetic state is unstable with respect to the onset of ferromagnetism, and in this case in the vicinity of the point $\zeta = 0$ the total energy is a decreasing function of magnetic moment ζ. Finding the *equilibrium* value of magnetic moment requires finding a solution of

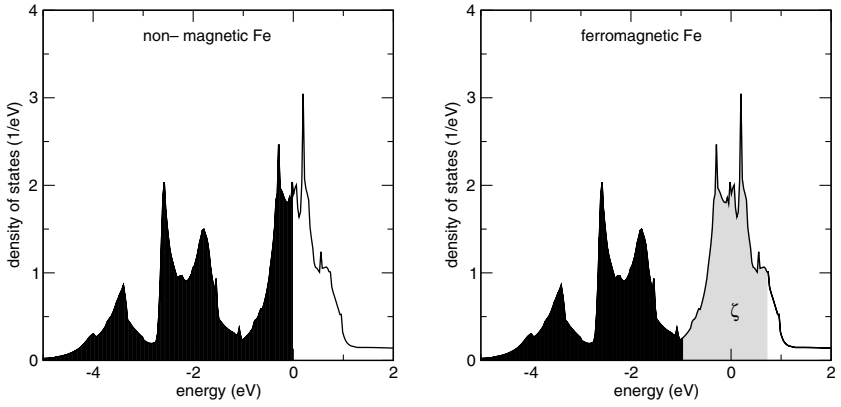

Fig. 1. The projected on-site densities of 3d-states of bcc iron found using the density functional full-potential linearized muffin-tin orbital (FP LMTO) approach [6]. In bcc iron the 3d-band contains approximately $N = 6.57$ d-electrons per atom. The Fermi energy of the non-magnetic state (left panel) corresponds to the origin of the energy axis. In the ferromagnetic symmetry-broken state (right panel) there are more electrons in the spin-up sub-band (grey) than electrons in the spin-down sub-band (black). The total area under the curve filled in grey colour equals the magnetic moment per atom ζ.

the full set of integral Eqs. (1)–(3) corresponding to the minimum of total energy (1). By repeatedly differentiating Eq. (1) we find that this equilibrium solution (corresponding to a ferromagnetic state) is defined by the three conditions [1,2]

$$\begin{aligned} &D(\epsilon_{\mathrm{F}})I > 1, \\ &\frac{I}{\epsilon_{\mathrm{F}\uparrow}-\epsilon_{\mathrm{F}\downarrow}}\int_{\epsilon_{\mathrm{F}\downarrow}}^{\epsilon_{\mathrm{F}\uparrow}} D(E)\,\mathrm{d}E = 1 \\ &I\left\{\frac{1}{2}\left[\frac{1}{D(\epsilon_{\mathrm{F}\uparrow})}+\frac{1}{D(\epsilon_{\mathrm{F}\downarrow})}\right]\right\}^{-1} < 1. \end{aligned} \tag{5}$$

The first equation is the condition of instability of the *non-magnetic* state, the second derives from the fact that at a minimum point $\partial E_{\mathrm{tot}}/\partial\zeta = 0$. The third condition follows from the fact that at a minimum the second-order derivative of the total energy $\partial^2 E_{\mathrm{tot}}/\partial\zeta^2$ must be positive.

The derivation of the functional form of the many-body magnetic interatomic potential uses Eq. (1), and is based on the assumption [7] that the density of states scales as a function of the local bandwidth W as $D(E) = W^{-1}F(E/W)$. The local bandwidth W is proportional to the square root of the pair-wise density term ρ, which in our case has the same meaning as in the Finnis–Sinclair potential model [8]. Using this approach, we find the following functional expression for the embedding part of the magnetic many-body interatomic potential [1]

$$F[\rho] = -A\sqrt{\rho} - \frac{B}{\ln 2}\left(1-\sqrt{\frac{\rho}{\rho_{\mathrm{c}}}}\right)\ln\left(2-\frac{\rho}{\rho_{\mathrm{c}}}\right)\Theta(\rho_{\mathrm{c}}-\rho), \tag{6}$$

where ρ_{c} is the critical value of the effective density ρ at which magnetic moment vanishes, and $\Theta(x)$ is the Heaviside function, $\Theta(x) = 1$ for $x > 0$ and $\Theta(x) = 0$ for $x < 0$. The magnetic moment per atom is given by a power-law approximation of the form [2]

$$\zeta = C\left(1-\sqrt{\frac{\rho}{\rho_{\mathrm{c}}}}\right)^{\gamma}, \tag{7}$$

where C and γ are adjustable parameters chosen to reproduce the *ab-initio*-derived bulk bcc moment behaviour as a function of volume per atom. The numerical values for the C and γ parameters corresponding to case study II of parametrization of the potential [1] are, respectively, 2.929 μ_{B} and 0.259, resulting in an equilibrium bulk magnetic moment of 2.154 Bohr magnetons.

3. Magneto-elastic fields and thermal migration of interstitial defects

Density functional calculations [9] show that magnetic moments near the core of an interstitial atom defect are very different from the bulk equilibrium value. Within the framework of the magnetic potential formalism, we are able to relate the calculated value of the effective pairwise density function ρ on an atom to the magnitude (but not to the direction) of magnetic moment (7) of the atom [2]. This approach has recently been extended to include the treatment of precession of directions of magnetic moments at a finite temperature [10]. In this paper we perform atomistic simulations using Eq. (6), which provides information not only about the non-magnetic and magnetic parts of the potential energy of every atom forming a defect configuration, but also about the distribution of the magnitude of magnetic moments in the configuration. Fig. 2 shows distributions of magnetic moments around $\langle 1\,1\,1\rangle$, $\langle 1\,1\,0\rangle$ and $\langle 1\,0\,0\rangle$ single self-interstitial atom (SIA) defects. Magnetic moments are suppressed in the regions of large compressive strain in the core of the defects, and magnetism is enhanced in the regions of tensile strain around the defects.

The advantage of using a semi-empirical molecular dynamics approach to evaluating magnetic moments in a locally deformed ferromagnetic material becomes particularly evident if we consider a large dislocation loop. At present it is still computationally too expensive to apply density functional methods to systems containing more than ~500 iron atoms, while investigating the distribution of magnetic moments around a mesoscopic dislocation loop in iron requires using a simulation cell containing approximately a million atoms. Fig. 3 shows the distribution of magnetic moments in the vicinity of $\langle 1\,1\,1\rangle$ and $\langle 1\,0\,0\rangle$ interstitial dislocation loops. The simulations were performed using supercells containing 877952 atoms. They show that magnetism is enhanced in the regions where atoms are under tension (around the perimeter of a loop) and is suppressed in the regions of compressive strain within the glide prism of a loop. On average the presence of interstitial defects in iron suppresses magnetic moments. Indeed, the curve describing how a magnetic moment ζ depends on volume per atom V is strongly asymmetric [11,2], and the increase of magnetic moment in the limit of large V (in the regions of tensile strain) does not compensate the rapid collapse of the moment in the limit of small V

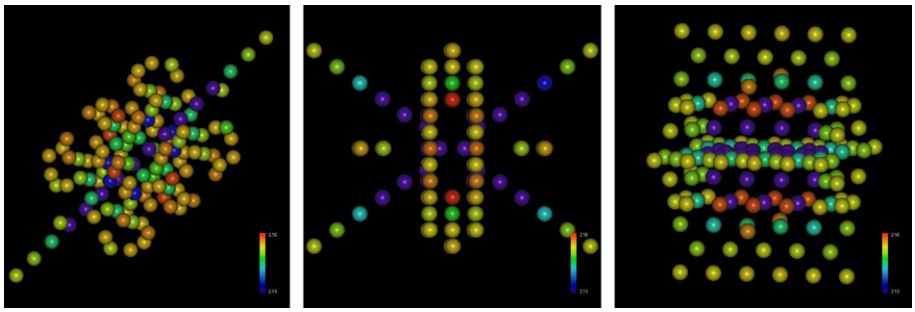

Fig. 2. Distribution of magnetic moments around a ⟨1 1 1⟩ (left panel), ⟨1 1 0⟩ (centre), and ⟨1 0 0⟩ (right panel) single self-interstitial atom defect. The atoms shown in the images have potential energy greater than −4.315 eV, exceeding by 0.001 eV the potential energy of an atom in a perfect lattice. The colour refers to the value of magnetic moment on an atom, where blue represents a moment equal to or less than 2.13 μ_B and red a moment equal to or greater than 2.16 μ_B. The equilibrium value of magnetic moment in a perfect bcc crystal lattice is assumed to be 2.154 μ_B [11]. In all the figures the vertical axis is parallel to the 0 0 1 direction, and the defect configurations were rotated around this axis to help visualize their structure. (For interpretation of the references to color in this figure legend, the reader is referred to the web version of this article.)

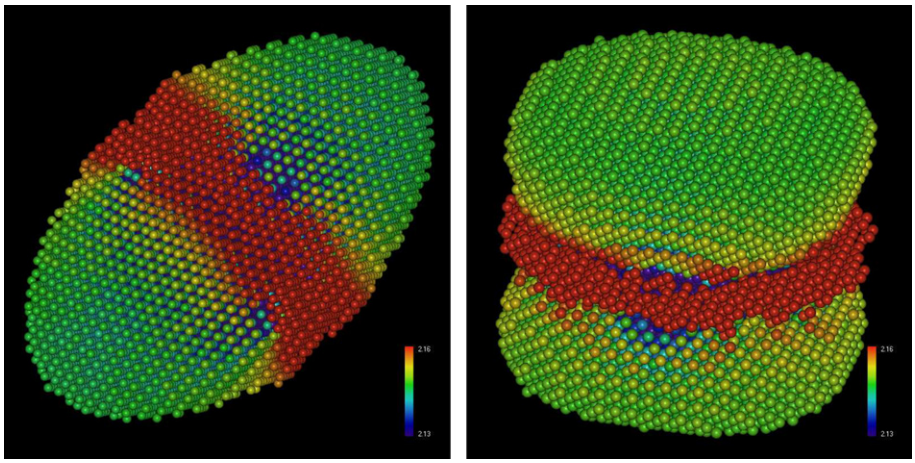

Fig. 3. Distribution of magnetic moments around a 253-atom ⟨1 1 1⟩ (left panel) and around a 304-atom ⟨1 0 0⟩ (right panel) interstitial dislocation loop. The similarity between the distribution of magnetic moments around a ⟨1 0 0⟩ loop and a hamburger is accidental. The atoms shown in the images have potential energy greater than −4.315 eV (i.e. the potential energy of an atom shown in the figure exceeds by 0.001 eV the potential energy of an atom in a perfect lattice), and the colour refers to the magnitude of magnetic moment of an atom. Blue represents a moment equal to or less than 2.13 μ_B and red a moment equal to or greater than 2.16 μ_B. The model equilibrium value of magnetic moment in a perfect bcc crystal lattice is 2.154 μ_B. (For interpretation of the references to color in this figure legend, the reader is referred to the web version of this article.)

occurring in regions of compressive strain. The prediction that interstitial atom clusters and dislocation loops are in effect regions of low magnetic moment can probably be verified experimentally using small-angle neutron scattering (SANS).

In Refs. [1,2] we investigated the pathway of migration of a *single* interstitial atom defect and found that the activation energy for migration was ~0.32 eV, in good agreement with *ab-initio* calculations [12]. Molecular dynamics simulations performed using earlier versions of empirical potentials [13] predicted that migration of *clusters* of self-interstitial atoms containing more than one interstitial atom was characterized by fairly low activation energies of the order of 0.025 eV. Density functional calculations [12], on the other hand, suggest that clusters containing up to three self-interstitial atoms adopt the ⟨1 1 0⟩-like configurations characterized by low thermally activated mobility. We carried out molecular dynamics simulations of migrating self-interstitial clusters containing up to seven self-interstitial atoms. Simulations were performed at $T = 50$ K and extended up to 1 ns. We found that many of the clusters containing

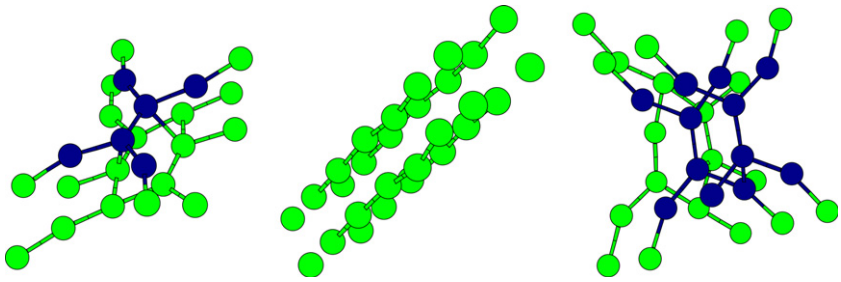

Fig. 4. Examples of a three-interstitial (left panel) and four-interstitial (centre and right panels) atom cluster configurations simulated using constant-temperature molecular dynamics at $T = 50$ K. The $\langle 1\,1\,0\rangle$ groups responsible for the reduced mobility of the clusters are highlighted by a darker colour. All the atoms forming these structures have a potential energy that exceeds by 0.1 eV the average potential energy of atoms in the lattice. The compact four-interstitial cluster (centre) has a rhombus shape if viewed in the $\langle 1\,1\,1\rangle$ direction. It retains its linear configuration in the limit $T \to 0$.

four or fewer self-interstitial atoms eventually collapsed into relatively immobile configurations containing $\langle 1\,1\,0\rangle$-like groups of atoms. Examples of configurations adopted by some of the three- and four-interstitial atom clusters found in our simulations are shown in Fig. 4. Only very compact clusters (for example a rhombus-shaped four-interstitial cluster) adopted linear $\langle 1\,1\,1\rangle$-crowdion configurations and continued migrating one-dimensionally at low temperatures [14]. The effective activation energy E_a for Brownian motion of $\langle 1\,1\,1\rangle$ crowdions forming the cluster was determined using the nudged elastic band model. Using the magnetic potential [1] we found that $E_a \sim 0.05$ eV.

This observation has significant implications for the interpretation of experimentally observed resistivity recovery curves of bcc iron. Clustering of self-interstitial atoms in cascades in neutron-irradiated or ion-irradiated iron [15] (as opposed to iron irradiated by electrons, where the probability of clustering of self-interstitial atoms is relatively low) will likely result in the formation of a significant fraction of self-interstitial atom clusters exhibiting high mobility at low temperatures, as well as to the formation of nearly immobile clusters similar to those shown in Fig. 4. The presence of self-interstitial atom clusters that retain mobility at very low temperatures should give rise to resistivity recovery stages at temperatures significantly lower than the temperature of stage I ($\sim$120 K) corresponding to the onset of mobility of single-interstitial atom defects.

Given that the migration energy (0.32 eV) of a single-interstitial atom defect corresponds to a resistivity recovery stage at $\sim$120 K, the activation energy of $\sim$0.05 eV characterizing thermal migration of glissile self-interstitial atom clusters should be expected to give rise to a recovery stage at $T \sim 20$ K. Low-temperature recovery stages are well documented in the case of non-magnetic bcc metals [16], and a stage at $T = 23$ K was in fact observed in electron-irradiated pure iron [17].

We note that identifying recovery stages in iron at low temperatures will likely require a great deal of care since the generation of highly mobile self-interstitial clusters under low-temperature irradiation is going to be accompanied by the generation of effectively immobile single-interstitial atom defects and vacancies acting as pinning centres for migrating self-interstitial clusters. Still, we anticipate that a study of complex kinetics of interaction between defects formed under low-temperature irradiation will help understanding the microscopic origin of clustering of self-interstitial atom defects in high-energy neutron collision cascades occurring under neutron irradiation in ferromagnetic iron and iron-based steels and alloys.

Acknowledgements

We are grateful to H. Van Swygenhoven, I. Cook and J.W. Connor for their encouragement and support of this work. Work at UKAEA was funded by the UK Engineering and Physical Sciences Research Council (EPSRC), by the EXTREMAT integrated project and by EURATOM. This work was also supported by travel grants provided to the authors by the EURATOM staff mobility programme.

References

[1] S.L. Dudarev, P.M. Derlet, J. Phys. Condens. Matter. 17 (2005) 7097.
[2] P.M. Derlet, S.L. Dudarev, Prog. Mater. Sci. 52 (2007) 299.

[3] H. Hasegawa, D.G. Pettifor, Phys. Rev. Lett. 50 (1983) 130.
[4] E.C. Stoner, Proc. Roy. Soc. Lond. Ser. A 169 (1939) 339;
E.P. Wohlfarth, Rev. Mod. Phys. 25 (1953) 211;
D.M. Edwards, E.P. Wohlfarth, Proc. Roy. Soc. A 303 (1968) 127;
D.G. Pettifor, J. Magn. Magn. Mater. 15–18 (1980) 847;
D.G. Pettifor, Acta Mater. 51 (2003) 5649.
[5] L.D. Landau, E.M. Lifshitz, Statistical Physics, 3rd ed., Pergamon, Oxford, 1980.
[6] S.Y. Savrasov, Phys. Rev. B 54 (1996) 16470.
[7] G.J. Ackland, M.W. Finnis, V. Vitek, J. Phys. F: Metal Phys. 18 (1988) L153.
[8] M.W. Finnis, J.E. Sinclair, Philos. Mag. 50 (1984) 45;
M.W. Finnis, Interatomic Forces in Condensed Matter, Oxford University, Oxford, 2003.
[9] C. Domain, C.S. Becquart, Phys. Rev. B 65, art. No. 024103 (2001).
[10] P.W. Ma, C.H. Woo, S.L. Dudarev, in: Proceedings of EUROMAT 2007 conference, Nuremberg, Germany.
[11] V.L. Moruzzi, P.M. Marcus, P.C. Pattnaik, Phys. Rev. B 37 (1988) 8003.
[12] C.-C. Fu, F. Willaime, P. Ordejón, Phys. Rev. Lett. 92, art. No. 175503 (2004).
[13] Yu. N. Osetsky, D.J. Bacon, A. Serra, B.N. Singh, S.I. Golubov, Philos. Mag. 83 (2003) 61.
[14] A. Serra reported a similar observation at a meeting of the PERFECT integrated project, Saclay, October 2005.
[15] C.H. Woo, B.N. Singh, Philos. Mag. 65 (1992) 889.
[16] Landolt-Börstein, in: H. Ullmaer (Ed.), Numerical Data and Functional Relationships Science and Technology, Atomic Defects in Metals, vol. 25, Springer-Verlag, Berlin, 1991, p. 115.
[17] S. Takaki, J. Fuss, H. Kugler, U. Dedek, H. Schultz, Radiat. Eff. 79 (1983) 87.